IOP Conf. Series: Journal of Physics: Conf. Series **918** (2017) 012037 doi:10.1088/1742-6596/918/1/012037

Simulation of droplet impact onto a deep pool for large Froude numbers in different open-source codes

V N Korchagova[1,2], M V Kraposhin[1], I K Marchevsky[1,2], E V Smirnova[1,2]

[1]Institute for System Programming of Russian Academy of Sciences, Alexander Solzhenitsyn st. 25, Moscow, 109004 Russian Federation
[2]Bauman Moscow State Technical University, 2-ya Baumanskaya st. 5, Moscow, 105005 Russian Federation

E-mail: v.korchagova@ispras.ru, m.kraposhin@ispras.ru, iliamarchevsky@mail.ru, alena.davidova@ispras.ru

Abstract. A droplet impact on a deep pool can induce macro-scale or micro-scale effects like a crown splash, a high-speed jet, formation of secondary droplets or thin liquid films, *etc*. It depends on the diameter and velocity of the droplet, liquid properties, effects of external forces and other factors that a ratio of dimensionless criteria can account for. In the present research, we considered the droplet and the pool consist of the same viscous incompressible liquid. We took surface tension into account but neglected gravity forces. We used two open-source codes (OpenFOAM and Gerris) for our computations. We review the possibility of using these codes for simulation of processes in free-surface flows that may take place after a droplet impact on the pool. Both codes simulated several modes of droplet impact. We estimated the effect of liquid properties with respect to the Reynolds number and Weber number. Numerical simulation enabled us to find boundaries between different modes of droplet impact on a deep pool and to plot corresponding mode maps. The ratio of liquid density to that of the surrounding gas induces several changes in mode maps. Increasing this density ratio suppresses the crown splash.

1. Introduction

Simulation of droplet impact hydrodynamics is a key element in a number of technological studies. Droplet impact simulation is important in such areas as ink-jet printing, internal combustion engine design and optimization, microchip manufacturing, solving meteorological problems and many others. However, numerical simulation of droplet impacts (considering flows with a free surface) is a complicated problem because high accuracy is critical for correct simulation of different phenomena arising after droplet impact. A suitable numerical algorithm should satisfy general requirements like numerical stability, convergence, low dissipation rate in the proximity of the liquid free surface, etc.

Worthington published the first studies of droplet impact onto a liquid layer in the late 19th century. Now there exist many papers on experimental and numerical studies in this area. The most popular ones deal with droplet impact on a deep pool [1, 2, 3], on a thin liquid film [1, 4, 5] or on a liquid layer whose depth is of the same order as the droplet diameter [6], and with droplet impact onto a dry solid surface, both hydrophilic and hydrophobic [1, 4, 7]. There are also some experimental results

regarding thermal convection and the effect of other factors (for example, a magnetic field) on the behaviour of the liquid after the impact [1].

Different post-impact phenomena may appear, such as secondary droplet formation, crown splashing, high-speed jets. It appears reasonable to introduce a ratio of dimensionless criteria to correlate the differences between impact modes. This approach allows us to point out the degree of effect that different physical processes may have on the behaviour of the liquid after the impact in each case. Therefore, the main question is how the values of dimensionless criteria are related to appearance or suppression of different phenomena.

There are several known papers featuring in-depth research on this problem. They present mode maps for the phenomena mentioned, plotted depending on the ratio of dimensionless criteria [2, 5]. The authors of these works considered various ranges of dimensionless criteria for droplet impact on a deep pool or on a thin liquid layer, but they did not focus on droplet behaviour in a number of 'extreme' modes, i.e. when the values of dimensionless criteria are very large. For example, from the practical point of view it is interesting to consider droplet behaviour if the gravity force effect vanishes (when the Froude number value is over 105). Therefore, the main aim of our research is to plot mode maps for droplet impact on a deep pool under this assumption.

There exist two ways to investigate this problem: experimentally and by means of numerical simulation. However, for the 'extreme' modes mentioned it is sometimes impossible (or hardly possible) to perform precise experiments, so numerical simulation is preferable. Moreover, numerical studies allow researchers to vary problem parameters independently, which is difficult in an actual experiment.

Since code development is a very labour-intensive and time-consuming procedure even in the case of well-known problems, usage of open-source numerical codes is widespread. While some open-source codes may be based on nearly the same numerical methods, specific algorithms implemented in them may differ significantly, and as a result, it leads to differences in approximation properties, dissipation rate, numerical stability, etc. Therefore, it is interesting to compare numerical simulation results of several open-source codes and find the area where the results are in good agreement. We used two codes in this study, OpenFOAM and Gerris, which fully implement numerical models used to simulate the physical phenomena that interest us.

2. Governing equations

Consider a droplet of viscous incompressible liquid, the droplet diameter being d. The droplet falls vertically onto a deep pool (figure 1); the liquid in the pool is the same as in the droplet. We assume the pool depth H and length L to be infinitely large (with respect to the droplet diameter). U is impact velocity. The densities and dynamic viscosity coefficients of the liquid and the gas above the pool surface are ρ_f, μ_f and ρ_a, μ_a, respectively. The gravitational acceleration is $\vec{g}$; the surface tension coefficient is σ.

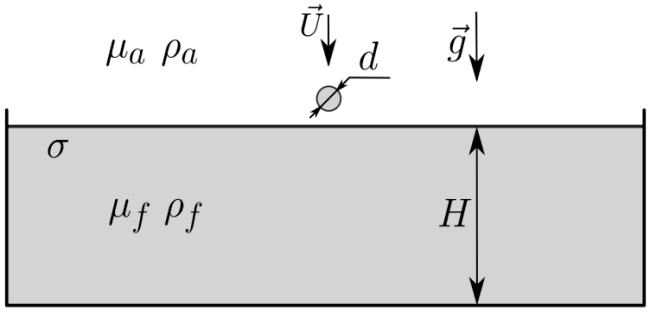

Figure 1. Problem statement. A droplet falling vertically into a deep pool

The governing equations are the continuity equation and the Navier — Stokes equations (mass and momentum conservation for incompressible Newtonian fluids):

$$\nabla \cdot \vec{U} = 0;$$

$$\frac{\partial \rho \vec{U}}{\partial t} + \left(\rho \vec{U} \cdot \nabla\right)\vec{U} = -\nabla p + \nabla \cdot \hat{\tau} + \rho \vec{g},$$

where p is pressure, $\hat{\tau} = \mu\left(\nabla \vec{U} + \nabla \vec{U}^T\right)$ is the viscous stress tensor.

Boundary conditions on the free surface between the liquid and surrounding gas should satisfy the surface energy balance and velocity continuity condition [8]:

$$\left(p_f - p_a\right)\vec{n} + \left(\hat{\tau}_f - \hat{\tau}_a\right) \cdot \vec{n} = \sigma \kappa \vec{n};$$

$$\vec{U}_f = \vec{U}_a.$$

Here $\vec{n}$ is a unit normal vector directed from the liquid into the gas; κ is the mean curvature of the interface. Introducing an additional force term into the momentum equations can automatically satisfy the first boundary condition [10].

We can write the governing equations down in a dimensionless form. We can use three dimensionless criteria to describe general properties of the case considered:

- Reynolds number $\mathrm{Re} = \rho U d / \mu$ defines the ratio of inertial forces to viscous forces;
- Weber number $\mathrm{We} = \rho U^2 d / \sigma$ is the ratio of inertial forces to surface tension;
- Froude number $\mathrm{Fr} = U^2 / (gd)$ shows the ratio of inertial forces to gravity.

3. Published results regarding droplet impacts

One way to classify the phenomena that appear after a droplet impact onto a deep pool is to divide them in two groups: large-scale and small-scale effects. Large-scale ones are crater and high-speed jet formation in the liquid after a droplet falls, secondary drops tearing off the top of the jet, and the crown splash [4]. All these phenomena have a common property: their characteristic scales are of the same order as the initial droplet diameter. Let us estimate the size of the mesh that is required to represent them correctly. For simplicity, we consider the mesh to be uniform; the resolution should be at least 20 cpd (cells per diameter). Our computational domain size should be on the order of $20d$ along each dimension; the initial position of the droplet is in the centre. Therefore, for 2D and axisymmetric simulations, the total number of cells is on the order of 10^5; 10^7 for a 3D case. Such meshes are acceptable for numerical simulation (in parallel mode), so simulating large-scale phenomena is feasible in principle. Mesh refinement procedures can significantly reduce the number of cells further. In this study, we investigate large-scale phenomena: the crown splash and high-speed jet formation.

We should note that small-scale phenomena (bubble entrapment, microdroplet splash and ejecta sheet at the moment when the droplet touches the pool surface [4, 5, 9]) are more difficult for numerical simulation. The mesh resolution required here is at least 200 cpd, so the only way to perform a simulation is to use adaptive mesh refinement.

A number of papers [2, 4, 5] attempted to predict appearance of large-scale effects as depending on physical properties of the liquid and gas as well as on droplet diameter and impact velocity. Such studies are mostly experimental and cover a small range of dimensionless criteria. Certain authors attempted to generalize previously published results and supplement them with experimental and numerical results of their own. Ultimately, they endeavoured to represent their results by plotting so-called mode maps.

An experimental study [5] considers a droplet impact on a thin liquid layer (of an approximately $0.2d$ depth). The authors fully investigated different types of crown effects, such as crown splash, microdroplet splash, ejecta sheet, Peregrine sheet, and obtained the diagram shown in figure 2. The

boundaries between different modes are clear. The authors assumed that it is possible to neglect the effect of gravity. For all cases, Froude numbers [5] are larger than 10^2 .

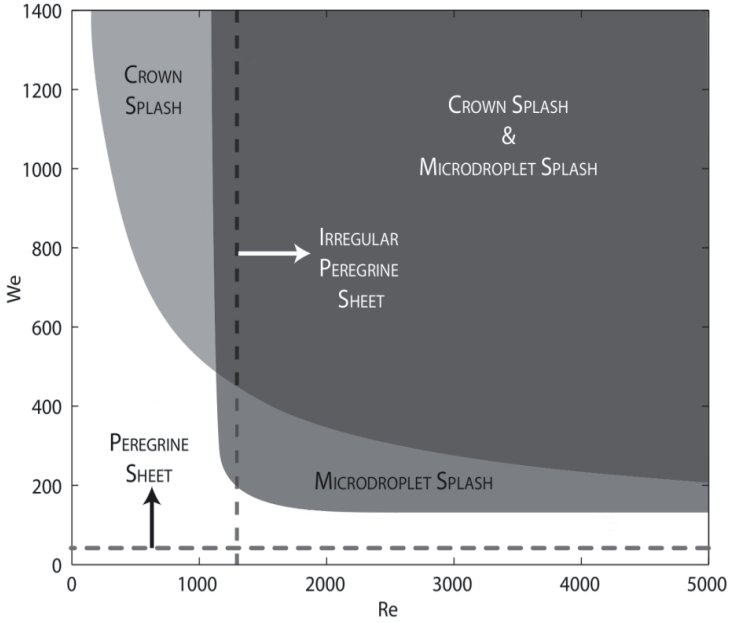

Figure 2. Mode map for crown effects after a droplet impact on a thin liquid layer [5]

Another large-scale phenomenon is high-speed jet formation. Authors of the paper [2] investigated shapes of high-speed jets being formed after a droplet impacts a deep pool (its depth was $7.2d$). Figure 3 shows a mode map from [2] for jet shapes depending on surface tension and gravity, with a Reynolds number of approximately 10^3 . This mode map presents joint results of experiments and OpenFOAM axisymmetric numerical simulations. The paper [2] states the results are in good agreement with experimental data. The authors compared empirical 'boundaries' for the Weber and Froude numbers corresponding to different modes from previously published experimental studies with the numerical results and noted that gravity forces and surface tension have a significant effect on the form of high-speed jets and the behaviour of liquid in general.

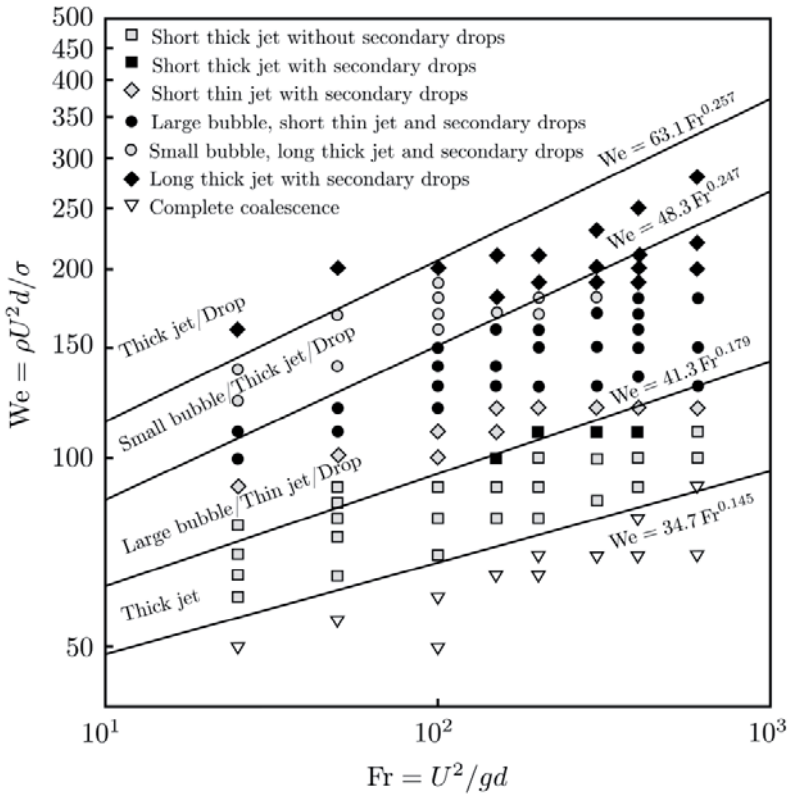

Figure 3. Mode map for high-speed jets after a droplet impact onto a deep pool, $\mathrm{Re} \approx 10^3$ [2]

Power functions can approximate plots of mode 'boundary' values. They do not have any asymptotes, but it is obvious that they exist because large values of dimensionless criteria mean that it becomes possible to neglect the corresponding forces as compared to inertial forces. For example, a large Froude number means that gravity is negligible. However, such modes are interesting in practice because they appear in the cases of very small droplets (with diameters of about a few micrometers) when impact velocity is rather high (over 100 m/s). These cases are common in ink-jet printing, microchip manufacturing, *etc*.

We consider gravity forces to be negligible if the Froude number exceeds a certain critical value, close to 10^5. We found this value through a series of simulations in which we gradually decreased gravity values.

4. Tools and numerical schemes

It is necessary to choose a suitable tool for numerical simulation. Different open-source codes can be used for scientific research, so we reviewed the degree to which these codes are applicable for the problem under consideration. According to the main aims of our investigation and our problem statement, correct surface tension models must be implemented in selected packages since surface tension forces play a crucial role in fluid behaviour.

As a result of comparing different codes, we chose two of them: OpenFOAM and Gerris. We also looked at some other codes, which are based on other numerical methods, like meshfree methods (for example, Smoothed Particle Hydrodynamics), hybrid methods (Particle Finite Element Method), immersed boundary methods. However, either these codes implement no surface tension models, or they need to be validated and/or modified significantly.

Both OpenFOAM and Gerris are based on the Finite Volume Method [10, 11]. The main idea is that, for the case of two media in the computational domain, governing equations are solved over the

whole domain for a 'mixture' with corresponding physical properties, *i.e.*, according to Volume of Fluid (VOF) approach [10, 11].

An additional variable is added to the model, a volume fraction function α_i of the i-th phase. It shows the ratio between the liquid and gas in the cells (usually the liquid is the 1st phase, gas is the 2nd phase):

$$\alpha_1 = \begin{cases} 1, & \text{in the liquid subdomain;} \\ 0, & \text{in the gas subdomain;} \\ (0, 1), & \text{in the proximity of the interface.} \end{cases}$$

It is obvious that for two phases

$$\alpha_1 + \alpha_2 = 1.$$

The transport equation for the volume fraction should be solved together with the continuity and momentum equations:

$$\frac{\partial \alpha_1}{\partial t} + \nabla \cdot (\vec{U}\alpha_1) + \nabla \cdot (\vec{U}_R \alpha_1 \alpha_2) = 0.$$

Here $\vec{U} = \alpha_1 \vec{U}_1 + \alpha_2 \vec{U}_2$ is the velocity of the mixture, $\vec{U}_R = \vec{U}_1 - \vec{U}_2$ is the relative velocity of the phases; there exist special discretization approaches to approximate it [10], making it possible to introduce a certain 'artificial' velocity which 'compresses' a subregion of the interface.

The volume fraction gradient approximates surface tension forces $\vec{f}_\sigma$ [12] considered as an additional term in the Navier — Stokes equations:

$$\vec{f}_\sigma \approx \sigma \kappa \nabla \alpha_1.$$

OpenFOAM and Gerris calculate mean interface curvature κ differently. OpenFOAM uses the gradient of the volume fraction function for curvature approximation:

$$\kappa \approx \nabla \cdot \left(\frac{\nabla \alpha_1}{\|\nabla \alpha_1\|} \right).$$

Gerris uses a level-set function to identify the interface [13]. For 2D simulations, an efficient algorithm exists to estimate curvature for a Cartesian mesh and a 7×3 stencil.

5. Discretization

The flow domain is axisymmetric, so in OpenFOAM we consider a 'wedge' with a single cell in the azimuthal direction with the corresponding boundary conditions on the sides of the wedge, and a flat region in Gerris. Artificial influence of the outer boundary conditions on the flow inside the domain should be as small as possible. Figure 4(a) shows the schematic of the flow domain and boundary conditions.

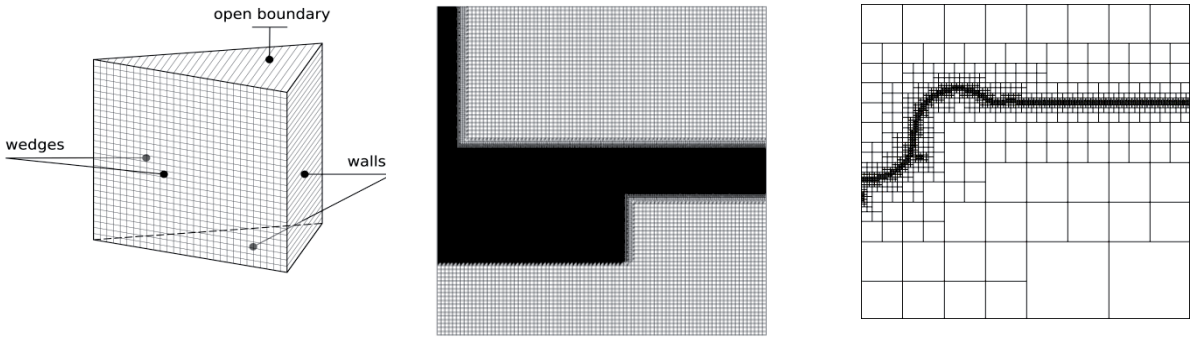

(a) (b) (c)

Figure 4. Discretization domain schematic: (a) schematic of boundary conditions; (b) sketch of a typical OpenFOAM mesh generated by the snappyHexMesh utility; (c) sketch of a dynamically refined mesh in Gerris

Mesh refinement technologies in OpenFOAM and Gerris differ significantly. In OpenFOAM, the mesh is static and the refinement is performed prior to calculations in the subdomains where the free surface can move during the solution process. In Gerris, the mesh is adaptively and dynamically refinable in the regions in the proximity of the interface (or in some other regions, if it is necessary).

Time step selection is automatic according to the value of the Courant-Friedrichs-Lewy (CFL) number. This approach makes it possible to obtain a numerically stable solution and provide a low level of non-physical disturbances.

6. Validation

We reviewed the information we found in previous publications dealing with validation of OpenFOAM and Gerris codes. Here we briefly describe the most interesting validation cases.

Validation test #1: Droplet impact and crown formation.

Paper [14] describes simulating a 3D droplet impact problem in OpenFOAM, using a mesh with 48 cells per diameter (48 cpd). We compared the results with experiments from [15] (figure 5).

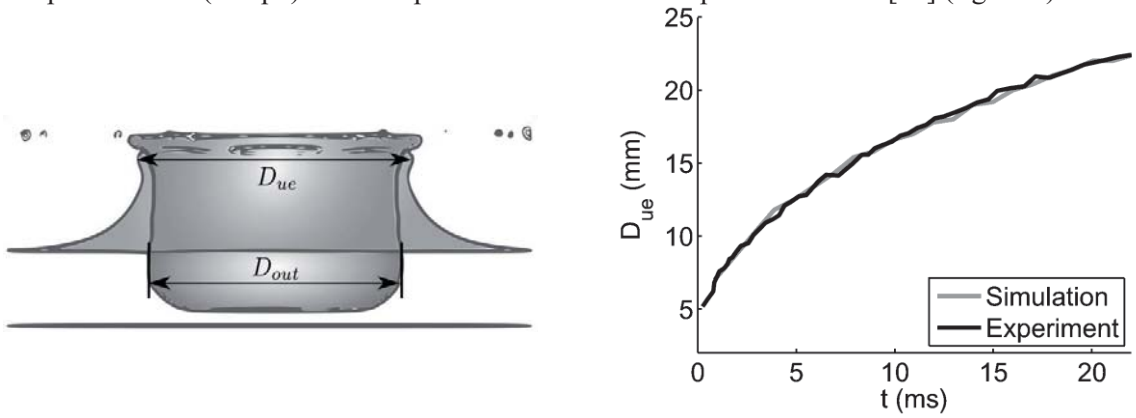

Figure 5. Comparison of droplet impact simulation from [14] with experimental data from [15]

Validation test #2: 2D standing capillary wave.

In the paper [14], the authors considered the problem of damping interface perturbation under surface tension and compared the kinetic energy from their OpenFOAM simulation with Lamb's analytical solution found in [16]. They also investigated mesh convergence and obtained good agreement between numerical and analytical solutions.

Validation test #3: Rayleigh breakup of a liquid jet.

An important feature of a Computational Fluid Dynamics code is the possibility of simulating instabilities. A well-known type of hydrodynamic instability is the Rayleigh — Plateau instability (breakup of a liquid jet). Paper [14] compares results of OpenFOAM simulation with a non-linear theory [17] that permits predicting size of droplets formed after jet breakup (figure 6 (a)). Results of simulation in Gerris were compared with linear Weber [18] and Rayleigh [19] theories that predict maximum and minimum jet radii (figure 6 (b)).

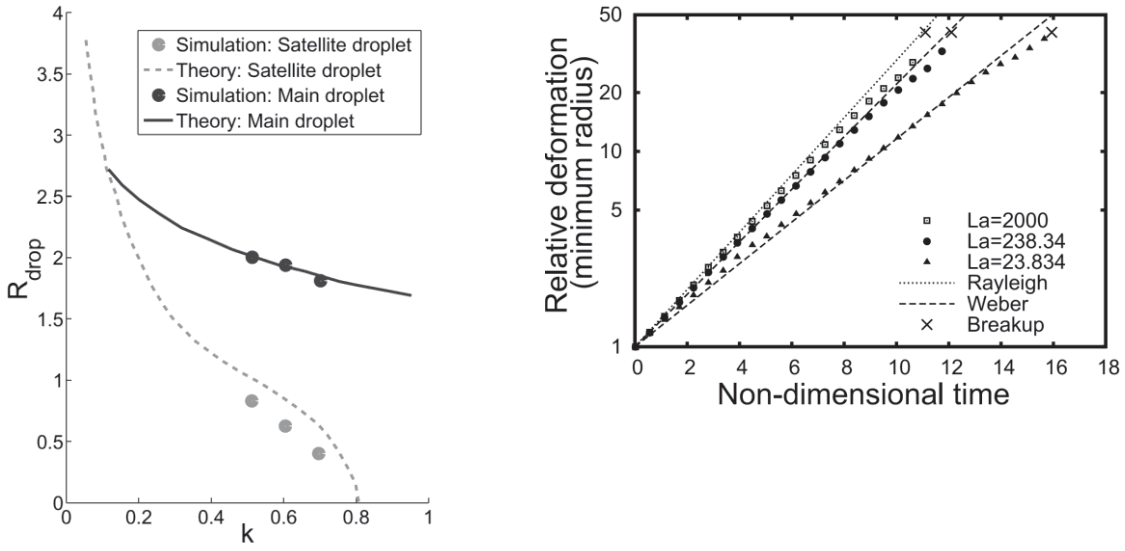

(a) (b)

Figure 6. Results of simulation of Rayleigh — Plateau instability: (a) OpenFOAM, comparison with non-linear theory; (b) Gerris, comparison with linear theory

Validation test #4: Retraction of a liquid column.
An initially stationary liquid column deforms under the action of surface tension. Results of 3D simulation in OpenFOAM (retraction of a cylindrical liquid column) [14] are compared with VoF results [20]. Mesh resolution is 32 cpd with respect to the column diameter. Paper [21] describes a similar case for Gerris, comparing the computed value of the so-called Taylor — Culick velocity with an analytical expression from [22]. There were 6×115 cells in the cross-section of the liquid region in the initial state (230 cpd).

Validation test #5: Kelvin — Helmholtz instability.
Paper [23] uses OpenFOAM to simulate the problem of Kelvin — Helmholtz instability, comparing the outcome with the numerical results of Rogers & Moser [24]. The authors noted that the results are in good agreement, but the paper does not present any quantified comparison results.

Validation test #6. Droplet deformation.
A droplet is placed in a gas flow and deforms with time. Results of OpenFOAM simulation [26] were compared with the theory of Stokes and Oseen [27], with the results of numerical simulations from [28] and the experiments of Temkin & Mehta [29].

Two numerical tests were performed to validate large-scale and certain small-scale phenomena simulation in OpenFOAM and Gerris.

Test #1. Large-scale phenomena.
We consider crater and high-speed jet formation in the axisymmetric case according to the paper of Berberović et al. [6]. In this paper, there are both experimental data and the necessary information about computational domain, mesh refinement and other key points for numerical simulation. Table 1 presents our input parameters.

Table 1. Input data for test 1 (for large-scale phenomenon validation).

Property	Value
Droplet diameter, d	2.67 mm

Impact velocity, U	2.56 m/s
Depth of the liquid layer, H	5.34 mm
Density of liquid, ρ_f	1179 kg/m^3
Dynamic viscosity of liquid, μ_f	$18.57 \cdot 10^{-3}$ Ns/m^2
Density of air, ρ_a	1.204 kg/m^3
Dynamic viscosity of air, μ_a	$1.9 \cdot 10^{-3}$ Ns/m^2
Surface tension coefficient, σ	0.063 N/m
Characteristic flow domain size, L	45 mm
Mesh refinement	30 cpd (cells per diameter)
CFL	0.2

Figure 5 shows the results of numerical simulation. To enable quantitative comparison of the results obtained, we measured two parameters at different time moments: crater depth (penetration depth) and crater diameter, measured halfway up the initial height of the liquid layer.

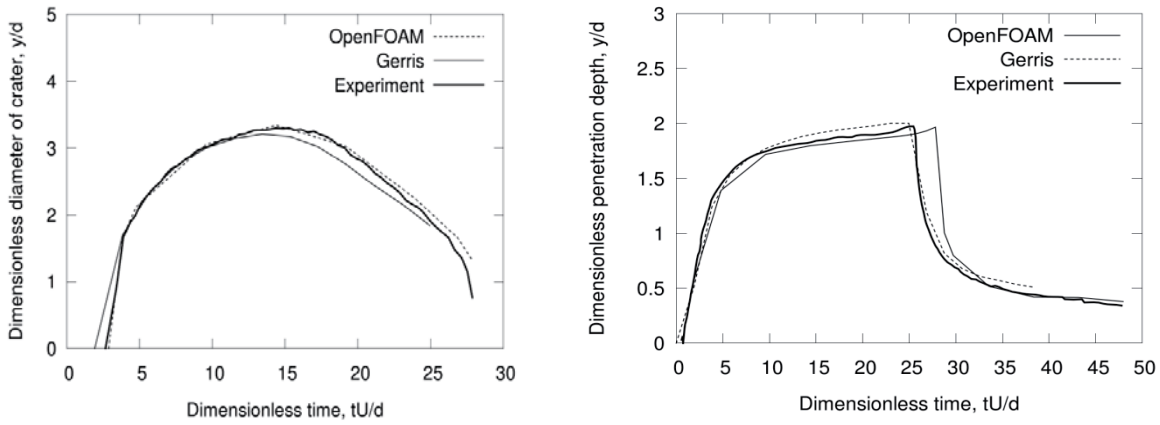

Figure 7. Comparison of experimental data with a numerical solution, test #1, Berberović et al. [6]: (a) crater diameter; (b) penetration depth

There is good agreement between experimental and numerical data. Therefore, mesh refinement over 30 cpd is enough to solve for large-scale effects correctly.

Test #2. Small-scale phenomena.

In paper [3], Tran et al. described an interesting small-scale phenomenon. When the falling droplet touches the surface of liquid, the bottom part of the droplet captures a thin film of air. This film keeps its 'continuous' shape for a short time and then it ruptures into a sequence of bubbles. There are experimental data for the penetration depth of the air film in this paper; therefore, this test makes for a good validation case. Table 2 shows our input data.

Table 2. Input data for test 2 (for small-scale effect validation).

Property	Value
Droplet diameter, d	1.9 mm
Impact velocity, U	0.55 m/s
Depth of the liquid layer, H	10 mm
Density of liquid, ρ_f	953 kg/m^3
Dynamic viscosity of liquid, μ_f	0.1906 Ns/m^2

Density of air, ρ_a	1.204 kg/m^3
Dynamic viscosity of air, μ_a	$1.9 \cdot 10^{-3}$ Ns/m^2
Surface tension coefficient, σ	0.0197 N/m
Characteristic flow domain size, L	45 mm
Mesh refinement	200 cpd (cells per diameter)
CFL	0.2

Figure 6 shows numerical simulation results for an air film penetrating a deep liquid pool. The $t = 0$ moment corresponds to the moment when the air film ruptures into bubbles. The quantitative results are in good agreement with the experimental data but the air film in the numerical solution turns into a bubble sequence shortly after the moment when the interaction between the droplet and the pool surface begins.

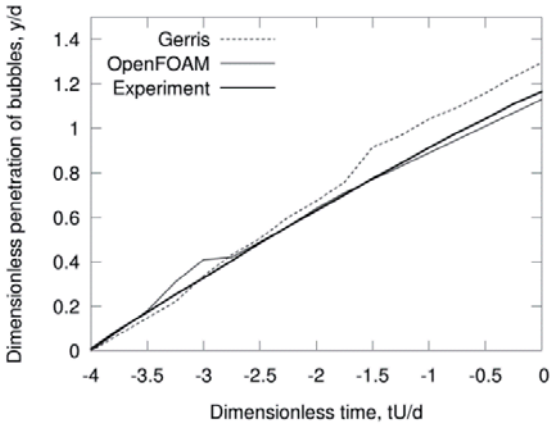

Figure 8. Penetration depth of the air film

7. Results and discussion

We note once again that we made the following assumptions for simulations in validation cases:

- the problems are considered to be axisymmetric because it is enough for correct simulation of crater and high-speed jets, and also can be useful for prediction of crown splash formation;
- mesh refinement was at least 20 (normally about 30) cells per diameter of initial droplet.

Post-impact behaviour of the liquid depends on the ratio between viscous forces, surface tension, inertial forces and external air pressure [30]. As for incompressible fluids, the main parameter is the pressure gradient, and during computations the pressure gradient can be defined by the liquid/gas density ratio δp.

In this study, we performed a series of computations in OpenFOAM and Gerris and obtained mode maps for two different values of the liquid/gas density ratio (figure 7–9). It is clear that increasing δp leads to suppression of modes featuring crown splashes and large drop formation on tops of high-speed jets. As for comparing computation results for these two open-source codes, the axisymmetric model in Gerris gives non-physical results in modes with the crown splash (when the Re and We numbers are large enough) — the secondary 'drops' pull to the centre of the flow region. It is the reason why we do not show these points on the Gerris mode maps.

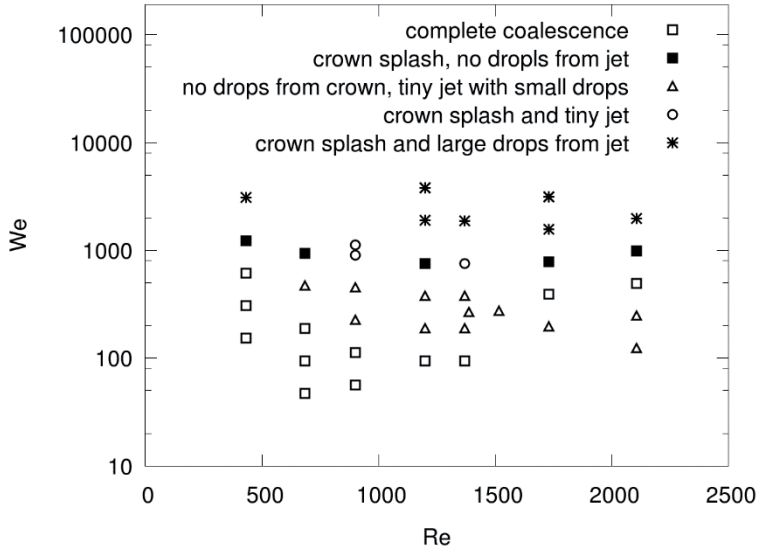

Figure 9. Mode map for droplet impact, generated from OpenFOAM results; the liquid/gas density ratio is 10^3

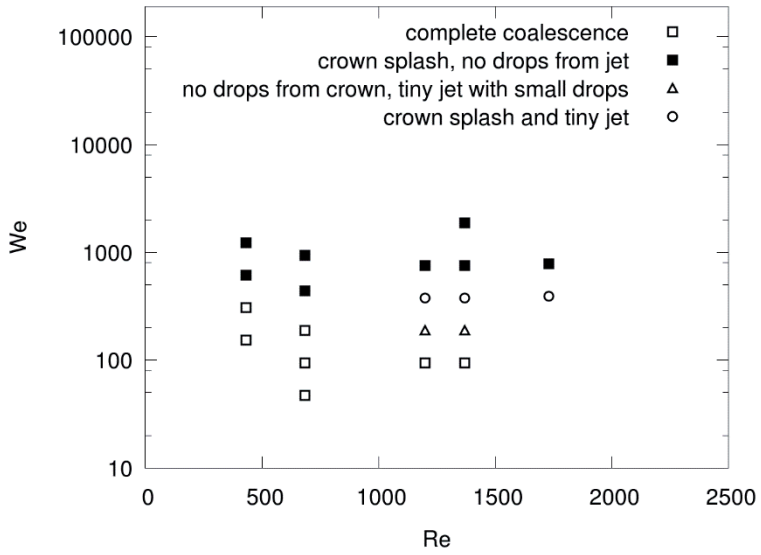

Figure 10. Mode map for droplet impact, generated from Gerris results; the liquid/gas density ratio is 10^3

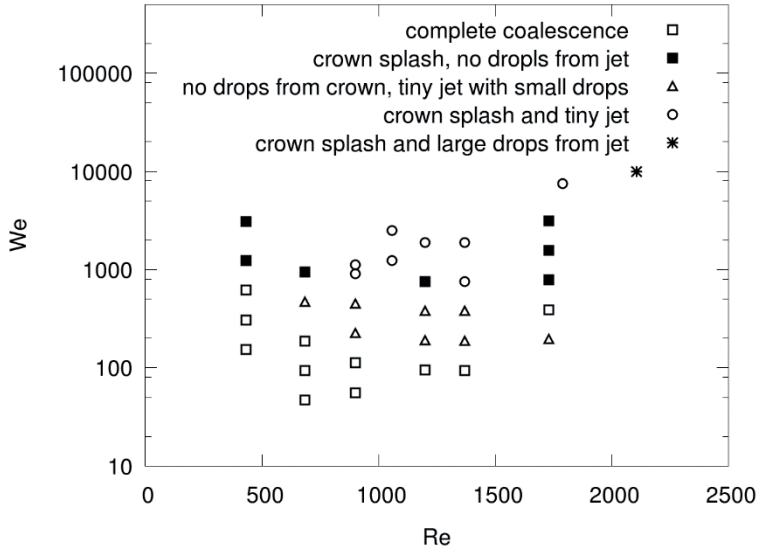

Figure 11. Mode map for droplet impact, generated from OpenFOAM results; the liquid/gas density ratio is 10^4

8. Conclusions

We investigated the problem of simulating a droplet impact onto a deep pool. First, we reviewed previously published results and analysed both experimental data and numerical results. Dimensionless criteria (Re, We, and Fr numbers) indicate ratios between various forces (inertia, surface tension, viscosity, gravity) and make it possible to predict droplet behaviour. Maps of various droplet impact modes can represent the results obtained.

Previous studies featured several maps for a number of specific modes in a small range of dimensionless criteria. Empirical functions for mode boundaries are power functions, but it is clear that certain 'saturation' values should exist. If the value of a dimensionless criterion exceeds a critical value, it means that it is possible to disregard the influence of the corresponding force, and the current mode position on the map will not change.

For example, low gravity conditions are of practical interest. Numerical investigation is the most convenient way to obtain mode maps because a full-scale experiment in these conditions is too difficult. It is important to use 'good' tools for simulation. We reviewed various open-source packages and chose two codes, OpenFOAM and Gerris. Various test cases helped us to validate these codes. We also found a lot of information relevant for code validation in published papers.

Numerical results of using these codes enabled us to plot mode maps. We considered the effect of the liquid-to-gas density ratio. Increasing it suppressed the crown splash. We obtained good agreement between maps for a high-speed jet. While we were able to predict results for a crown splash, it is necessary to run 3D simulations to obtain a correct solution.

Acknowledgements

The work of M.V. Kraposhin and I.K. Marchevsky is supported by the Russian Science Foundation (grant 17-79-20445).

References

[1] 2002 *Drop-Surface Interactions* (Berlin: Springer-Verlag) ed M Rein
[2] Ray B, Biswas G and Sharma A 2015 Modes during liquid drop impact on a liquid pool *J. Fluid Mech.* **768** 495–522
[3] Tran T, de Maleprade H, Sun C and Lohse D 2013 Air entrainment during impact of droplets on

liquid surfaces *JFM Rapids* **726** R3
[4] Yarin A I 2006 Drop Impact Dynamics: Splashing, Spreading, Receding, Bouncing... *Annu Rev. Fluid Mech.* **38** 159–92
[5] Deegan R D, Brunet P and Eggers J 2008 Complexities of splashing *Nonlinearity* **21**(1) C1
[6] Berberović E, van Hinsberg N P, Jakirlić S, Roisman I V and Tropea C 2009 Drop impact onto a liquid layer of finite thickness: Dynamics of the cavity evolution *Phys. Rev.* **79**
[7] Romanov A S and Semikolenov A V 2015 Film shape of partially wetting liquid while flowing down wetted surface *Vestn. Mosk. Gos. Tekh. Univ. im. N.E. Baumana, Estestv. Nauki [Herald of the Bauman Moscow State Tech. Univ., Nat. Sci.]* **5** 88–99
[8] Landau L D and Lifshitz E M 1959 *Fluid Mechanics, Volume 6 of A Course of Theoretical Physics* (New York: Pergamon)
[9] Zhang L V, Toole J, Fezzaa K and Deegan R D 2012 Evolution of the ejecta sheet from the impact of a drop with a deep pool *J. Fluid Mech.* **690** 5–15
[10] Rusche H 2002 *Computational Fluid Dynamics of Dispersed Two-Phase Flows at High Phase Fractions: Ph.D. thesis* (University of London, Imperial College)
[11] Ferziger J H and Perić M 2002 *Computational Methods for Fluid Dynamics* (Springer-Verlag)
[12] Brackbill J U, Kothe D B and Zemach C 1992 A Continuum Method for Modelling Surface Tension *J. Comput. Phys.* 100(2) 335–54
[13] Popinet S 2009 An accurate adaptive solver for surface-tension-driven interfacial flows *J. Comput. Phys.* **228** (16) 5838–66
[14] Deshpande S S, Anumolu L and Trujillo M F 2012 Evaluating the performance of the two-phase flow solver interFoam. *Comput. sci. disc.,* 2012 **5** (1)
[15] Cossali G E, Marengo M, Coghe A and Zhdanov S 2004 The role of time in single drop splash on thin film *Exp. Fluids* **36** 888–900
[16] Lamb H 1932 *Hydrodynamics* (New York: Dover)
[17] Lafrance P 1975 Nonlinear breakup of a laminar liquid jet *Phys.* Fluids **18** 428–32
[18] Weber C 1931 Disintegration of liquid jets *Zeitschrift fur Angewandte Mathematik und Mechanik* **11**(2) 136–59
[19] Rayleigh L 1892 On the instability of a cylinder of viscous liquid under capillary force *Phil. Mag.* **34**(207) 145–54
[20] Umemura A 2011 Self-destabilizing mechanism of a laminar inviscid liquid jet issuing from a circular nozzle *Phys. Rev.* **83**
[21] Fuster D, Agbaglah G, Josserand C, Popinet S and Zaleski S 2009 Numerical simulation of droplets, bubbles and waves: state of the art *Fluid Dyn. Res.* **41**(6)
[22] Savva N and Bush J W M 2009 Viscous sheet retraction *J. Fluid Mech.* **626** 211–40
[23] Wedolowski K, Bajer K and Kwiatkowski K 2011 Analysis and modelling of the effective reaction rate in a developing mixing layer *J. Phys.* **318**(9) 2688–97
[24] Rogers M M and Moser R D 1992 The three-dimensional evolution of a plane mixing layer: the Kelvin — Helmholtz rollup *J. Fluid. Mech.* **243** 183–226
[25] Orazzo A and Hoepffner J 2012 The evolution of a localized nonlinear wave of the Kelvin — Helmholtz instability with gravity. *Phys. Fluids*, **24**
[26] Jalaal M and Mehravara K 2014 Transient growth of droplet instabilities in a stream *Phys. Fluids* **26**
[27] Clift R, Grace J R and Weber M E 1978 *Bubbles, Drops and Particles* (Mineola: Dover Publ.)
[28] Quan S and Schmidt D P 2006 Direct numerical study of a liquid droplet impulsively accelerated by gaseous flow *Phys. Fluids* **18**, 102103
[29] Temkin S and Mehta H K 1982 Droplet drag in an accelerating and decelerating flow *J. Fluid Mech.* **116** (1) 297–313
[30] Xu L, Zhang W W and Nagel S R 2005 Drop Splashing on a Dry Smooth Surface. *Phys. Rev. Lett.* **94**, 184505